System Parameters Effect on the Turbulent Underwater Optical Wireless Communications Link

Zahra Vali[a,b,*], Asghar Gholami[a], Zabih Ghassemlooy[c] and David G. Michelson[b]

[a]*Department of Electrical and Computer Engineering, Isfahan University of Technology, Isfahan, Iran, 8415683111, gholami@cc.iut.ac.ir*
[b]*Department of Electrical and Computer Engineering, University of British Columbia, Vancouver, Canada, V6T 1Z4, zvali@ece.ubc.ca, davem@ece.ubc.ca*
[c]*Optical Communications Research Group, Faculty of Engineering and Environment, Northumbria University, Newcastle Upon Tyne, UK, NE1 8ST, z.ghassemlooy@northumbria.ac.uk*

Abstract

In underwater optical wireless communications (UOWC) the link performance is greatly affected by the turbulence. Turbulence is due to the random variations of the refractive index of water, which leads to both intensity (i.e., fading) and phase fluctuation of the optical beam. The effects of turbulence on link performance depend on the choice of system parameters. In this paper, the effects of the transmission link span, divergence angle of the transmitted Gaussian beam, receiver's (Rx) aperture diameter and field of view (FOV) on the UOWC link performance under the turbulence condition is investigated. The results show that, lognormal and negative exponential distributions fit well with the probability density function of the received light intensity under weak-to-strong and saturated turbulence regimes or for a link span longer than 120 m. The goodness of fit test is performed to validate the conformity of the two distributions with the simulation results. The scintillation index (SI) variation as a function of the four mentioned parameters under different turbulence regimes is investigated. It is shown that, for a 100 m link span and under weak turbulence, while the effect of transmitter's FOV on SI is negligible, increasing the transmitter's divergence angle by 1.72º and decreasing the Rx's aperture diameter by 9.2 cm, increases the SI by 53 times and 77 times, respectively.

* Corresponding author at: Department of Electrical and Computer Engineering, University of British Columbia, Vancouver BC V6T 1Z4, Canada. E-mail address: zvali@ece.ubc.ca

Keywords: underwater optical wireless communications; turbulence; probability density function; scintillation index

I. INTRODUCTION

Underwater optical wireless communications (UOWC) has attracted a great deal of attentions in recent years. For underwater communications, optical carriers in the blue-green wavelength bands experience the lowest power loss and offer higher modulation bandwidth compared to the acoustic and radio frequency (RF) based wireless technologies [1]. However, the environmental factors strongly affect the performance of UOWC systems. The most significant and well-studied environmental factors are the absorption and multiple scattering of lights and their impacts on the performance of UOWC links e.g., power loss, dispersion and bit error rate (BER) have been studied comprehensively [2]–[5]. In addition, the UOWC link performance is highly affected by turbulence in line with free space optical (FSO) communications in open air, which is extensively studied and reported in the literature [6]. However, in UOWC systems, experimental investigation of the turbulence effect on the link performance is much more challenging, thus the focus of most works reported are on system modelling and simulation [7]–[9].

A simple physical model representing a real underwater environment under different turbulence conditions based on Monte Carlo simulation was reported in [10]. In contrast to previous researches, where air bubbles, temperature, salinity gradient and eddy diffusivity ratio were used to characterize turbulence in UOWC [11]–[13], in [10] the transmission link span L and the refractive index variations Δn were used to investigate the received light intensity (i.e., by deriving the probability density functions (PDFs) and changes in the scintillation index (SI) under different turbulence regimes).

While lognormal distribution was adopted for weak and moderate turbulence regimes in [8]–[10], [14]–[18], based on our previous works on turbulence modelling [10], [19], in this paper we investigate the fluctuations of the received light intensity for a range of L and predict its PDF under the weak-to-strong and saturated turbulence regimes. Undertaking experimental test; measurements and evaluation under strong and saturated turbulence regimes, especially for long-range transmission links is a challenging task, therefore the focus of the work is based on the numerical and simulation investigations. We show that, fluctuations of the

received light intensity is best defined with the negative exponential distribution for saturated turbulence for longer transmission link spans (i.e., $L > 120$ m). Furthermore, we show that, how L, the divergence angle of the Gaussian beam at the Tx, the Rx's aperture diameter and its field of view (FOV) will influence the SI for a range of Δn, which has not been reported before.

This simulation work is based on the proposed model in [10], which was both verified with previous works and experimentally tested using a water pool under different turbulence conditions thus confirming the accuracy and feasibility of the simulation model [10], [19]. Besides, the accuracy of the eddy-based turbulence structure of the model was tested during implementation and argument as in [10] to show the conformance of the turbulence structure with narrow divergence beams. Furthermore, the effect of Rx's parameters i.e., FOV and aperture diameter on our simulation results is on the number of captured photons, which was tested and discussed in previous literature for practical scenarios. To the best of our knowledge, no practical implementation of UOWC with turbulence over long transmission links has been reported yet. The results presented here can be used as a primary step for further investigation of UOWC implementation in real scenarios.

The rest of the paper is organized as follows. The proposed PDF distributions and system model are described in Sections 2 and 3, respectively. Simulation results and discussions are outlined in Section 4. Finally, Section 5 concludes the paper.

II. PDF DISTRIBUTIONS

The atmospheric turbulence is categorized as weak, moderate, strong and saturated based on its strength [6]. There is no comprehensive single mathematical model for turbulence, which describes turbulence for all regimes; this is because of the complex nature of the environment. The three most widely adopted PDF distributions of the received light intensity in FSO systems for the weak, weak-to-strong and saturated regimes are lognormal, Gamma-Gamma and negative exponential, respectively. In this work, we consider both lognormal and negative exponential distributions of the received light intensity I, which are given by [6], [20]:

Lognormal

$$p(I) = \frac{1}{I\sigma_I\sqrt{2\pi}} \exp\left\{ -\frac{\left[\ln(\frac{I}{I_0}) + \frac{1}{2}\sigma_I^2 \right]^2}{2\sigma_I^2} \right\},\ I > 0 \tag{1}$$

$$\sigma_I^2 = \frac{\langle I^2 \rangle - \langle I \rangle^2}{\langle I \rangle^2}.$$

Negative exponential

$$p(I) = \frac{1}{I_0} \exp(-\frac{I}{I_0}),\ I > 0. \tag{2}$$

where I_0 is the mean received light intensity and σ_I^2 is the SI.

III. SYSTEM MODEL

A. Turbulence Model

Several factors e.g., movements of underwater vehicles can cause mixture of oceanic flows or flow perturbations, which leads to unstable turbulent flow primarily with large scale eddies [21]. In contrast to laminar flow, where the fluid moves uniformly in smooth layers with the same density, in turbulent flow the fluid undergoes irregular fluctuations or mixing and the density and velocity are not uniform. The result is the interaction of large-scale eddies with each other, dispersing their energy and forming smaller eddies [22], [23]. The chaotic nature of energy transfer from large to small eddies, creates homogeneous, isotropic, and steady turbulent eddies with different sizes and refractive indices *n* [6]. Therefore, to model turbulence the stratified water medium was assumed in the horizontal direction, where each layer represents a homogenous and an isotropic turbulent cell or eddy in the motion [10], [24]. Throughout the simulations runs, *n* of all cells are changing randomly to represent the variations of water's refractive index in both temporal and spatial domains.

B. Simulation Model

The model used in [10], which is based on the step-by-step tracing and interaction of propagating photons with the turbulent cells with different refractive indices and sizes from transmitter (Tx) to the (Rx), is adopted here as shown in Fig. 1. This is a Monte Carlo based simulation model for UOWC with turbulence in clear

water implemented in a horizontal point-to-point link along the z direction. The turbulent cells are defined within consecutive layers with width Δz on the z-axis, where θ_i and φ_i are the polar and radial angles chosen randomly between [0, θ_{max}] and [0, 2π], respectively with uniform distributions. This implies the rotation of curved boundaries along the z direction. The curved boundaries, which are assumed to be locally part of spheres with the radius R_i, and a normal vector $\vec{n}_i = (\sin\theta_i \cos\varphi_i, \sin\theta_i \sin\varphi_i, \cos\theta_i)$ separate the adjacent layers. Throughout the simulation, R_i is selected randomly from $R_i = |\log_e(q)|$, where q is a random number chosen uniformly within [0, 1]. With this assumption, smaller radius occurs more than larger ones, which is in accordance with natural situation and consequently, the focusing and defocusing effect of eddies is implemented on the laser beam. At the Tx side, the position and direction of each photon launched into the channel are determined. Photons are traced within channel by determining the intersection of each photon with each boundary and the new direction of a photon following refraction from the curved boundary is predicted using the three-dimensional Snell law. At every interaction of photons with the layers, their current positions and directions are updated and recorded, which are used at the Rx to make decisions on the received photons.

According to previous studies, n variation depends on the pressure P, temperature T, salinity S and wavelength λ, and it changes randomly and rapidly in turbulent dynamic underwater environments [23], [25], [26]. To simplify the model, we have accounted all the effective factors in n variation using a single parameter of Δn, which now can be used to indicate the turbulence strength. With this structure, Δn and L are the two important parameters, which affect the strength of turbulence as in [10]. It is assumed that, n varies in the interval of $[N_{avg} - \Delta n/2; N_{avg} + \Delta n/2]$, where N_{avg} is the average of the maximum variation of n within the range of 1.3412 to 1.3420 (max Δn = 8e-4), which is obtained from reported measured values for vertical profiles of temperature and salinity in Florida Strait using the refractive index equation reported in [23], [25]. Next, Δn is set independently for each scenario for different turbulence strengths, though generally any value of Δn can be selected. All the key system parameters considered in the model are listed in Table I.

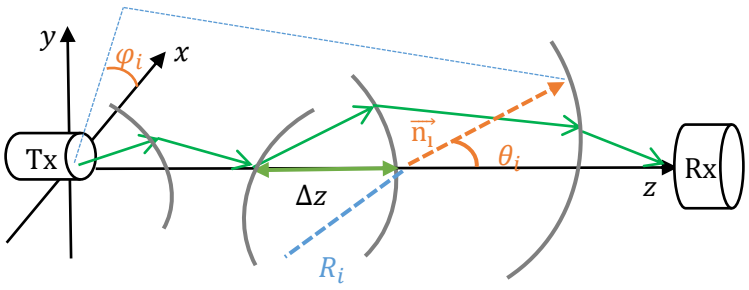

Figure 1. A schematic diagram of the system model consisting of the Tx, turbulent channel and the Rx

TABLE I. SYSTEM PARAMETERS

Section	Parameter	Value
Tx	Number of transmitted photons Wavelength Beam divergence angle (half angle) Root mean square beam width	1e5 520 nm 0.00075 rad 15 mm
Rx	Aperture diameter Aperture FOV	10 cm 180˚
Underwater channel	Link span Number of channel realizations Δn Δz θ_{max}	40, 80, 120, 150 m 1e3 8e-4 50 cm 45˚

IV. SIMULATION RESULTS

A. PDF Distributions

For a given value of Δn = 8e-4, Fig. 2 shows the PDF of the simulated received light intensity variation against the normalized intensity fitted with lognormal and negative exponential distributions for a range of L, the coefficient of determination R^2 and SI. Note that, the total number of received photons at the Rx for all 1e3 channel realizations were normalized to the average intensity I_0 and the SI values were obtained from (2). We did not consider longer link spans because of high attenuation of the light intensity especially beyond 200 m. Besides, scattering and turbulence will introduce additional attenuation and beam spreading. Fig. 2 shows deflection of the probability of received light intensity from lognormal for a link range of 150 m, which demonstrates the unpracticality of longer range UOWC systems.

As shown, there is a good fit between the lognormal and negative exponential distributions and the simulation results for the weak-to-strong and saturated turbulence regimes, respectively. Note, other reported

PDF distributions for strong atmospheric turbulence e.g., lognormal-rician, I-K, K and Gamma-Gamma distributions all tend to negative exponential distribution and therefore are not considered in this work [6].

In short range communication links, the number of received photons tend to fluctuate around the average value i.e., the probability of receiving average values is more and it tends to zero at both extreme sides (lognormal distribution). As the link range increases, the effect of turbulence on propagating photons is more evident, which results in more beam wandering and scintillation, consequently, fewer photons will arrive at the Rx. In other words, higher probability is observed around smaller values of intensity and vice versa (negative exponential).

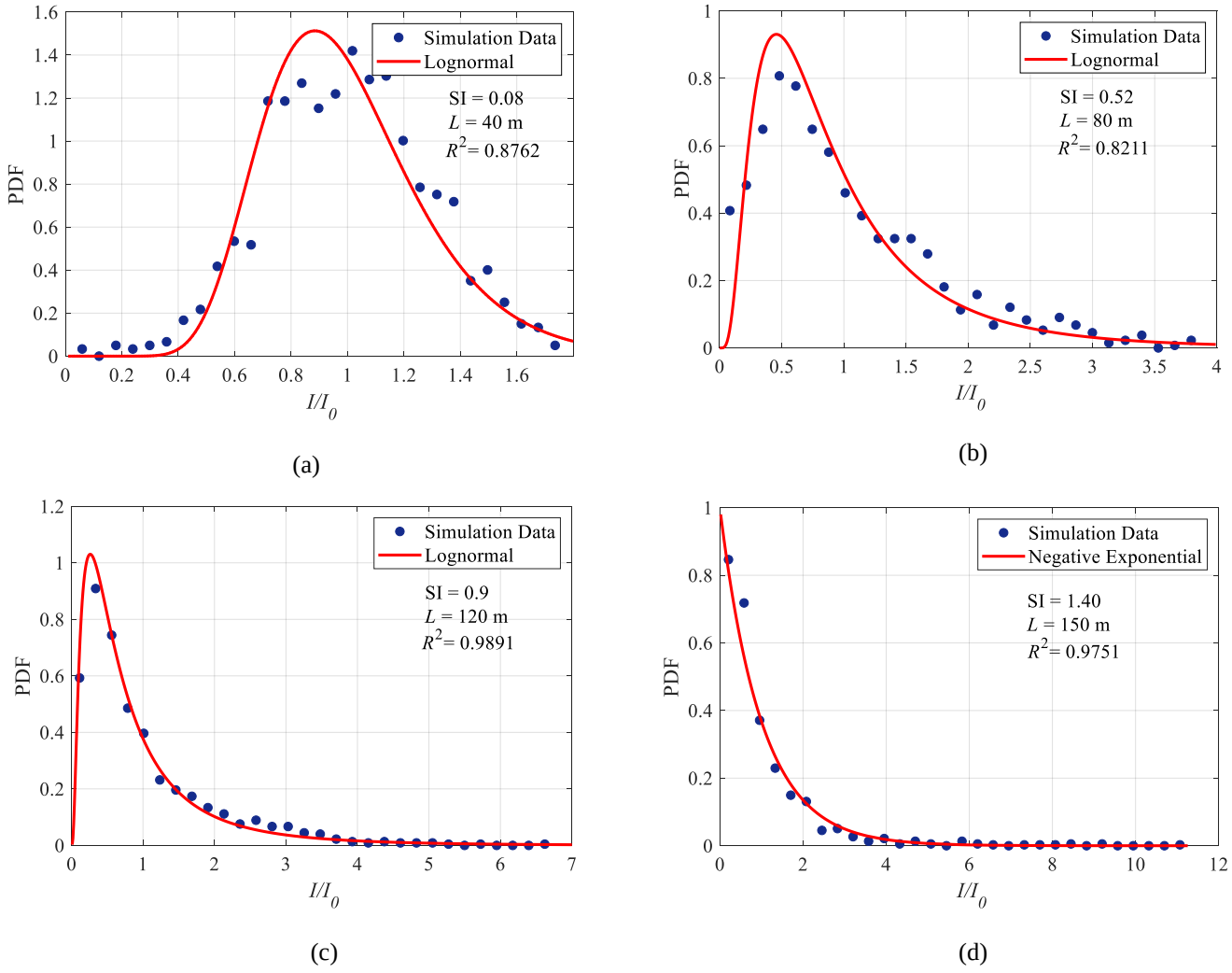

Figure 2. PDF of the simulated received light intensity vs. the normalized intensity fitted with lognormal and negative exponential distributions for: (a) L = 40 m, (b) L = 80 m, (c) L = 120 m and (d) L = 150 m

To evaluate how well the PDFs of simulation results fit with the lognormal and negative exponential distributions, we determine R^2 in order to perform the goodness of fit (GOF) test as given by [27]:

$$R^2 = 1 - \frac{\sum_{i=1}^{N} (x_i - y_i)^2}{\sum_{i=1}^{N} (x_i - \bar{x})^2} \tag{3}$$

where, N is the number of bins in the simulation distribution, x_i and y_i are the simulated and predicted values for the i^{th} intensity bin, respectively and $\bar{x}$ is the average of x_i. Generally, $0 < R^2 < 1$, where the upper value (i.e., 1) indicates a close fit between the results. R^2 values of 0.8762, 0.8211, 0.9891 and 0.9751 shown in Fig. 2 implies a good fit between the simulated data and selected formal distributions.

B. SI Variations

In this part, the impact of the divergence angle of Gaussian beam at the Tx output, Rx's aperture diameter, FOV and L on the SI are considered, respectively. Fig. 3 depicts the SI as a function of the Tx's divergence angle up to 1.72 º for a range of Δn and for L = 30 and 100 m, showing that SI increases with Δn. In long range communication links, the Gaussian transmitted beam with wider divergence angles leads to additional power attenuation. Thus, making Gaussian beams with wide divergence angles not practical for long range communication links.

For lower values of the divergence angles, the transmitted beam illuminates the center of the Rx (i.e., photodetector) and due to aperture averaging the turbulence effect is low. However, the SI increases with the divergence angle, due to more beam spreading and beam wandering, reaches the saturated (constant) level beyond the divergence angles of 0.57º and 0.29º for L = 30 and 100 m, respectively. The beam width w at the Rx can be estimated as $w \approx (f + L)\theta$, where $f \approx w_0/\theta$ is the focal length of the lens at the Tx, L is the link span, θ is half of the beam divergence angle and w_0 is the root mean square (RMS) beam width. For instance, θ = 0.75 º leads to $w \approx$ 31 cm and 101 cm for L= 30 m and 100 m, respectively. It is clear that for both link spans, $w >>$ the aperture radius (i.e., 5 cm), which reduces beam wandering effects and the SI values do not change any longer with the divergence angles.

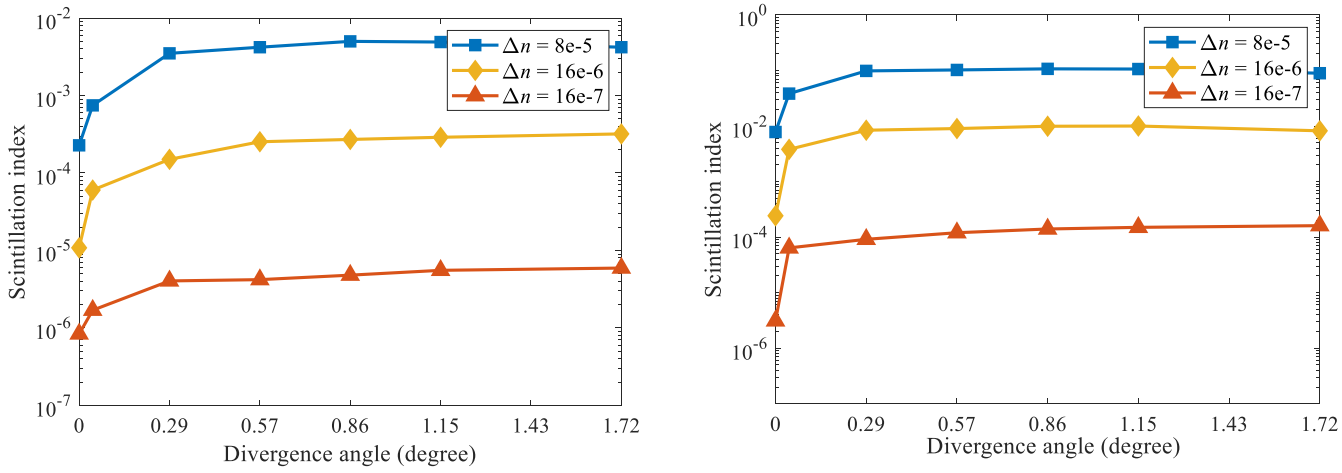

(a) (b)

Figure 3. SI vs. the Tx's divergence angle for different values of Δ*n*: (a) *L* = 30 m, and (b) *L* = 100 m

Fig. 4 shows the SI as a function of the Rx's aperture diameter for different values of Δ*n* and for *L* = 30 and 100 m. As shown, the SI decreases with the aperture diameter for all values of Δ*n* with lower values of Δ*n* displaying the lowest SI. E.g., for *L* = 100 m and Δ*n* = 16e-7, increasing the aperture diameter by almost ten times results in reduced SI by up to 77 times. Mitigating the random fluctuations of the received light intensity by increasing the aperture area is known as aperture averaging, which compensates for the scintillation and beam wandering effects [28]. It should be noted that, increasing the aperture area will also increase the background noise level, thus leading to lower signal to noise ratio, which is not considered in this work.

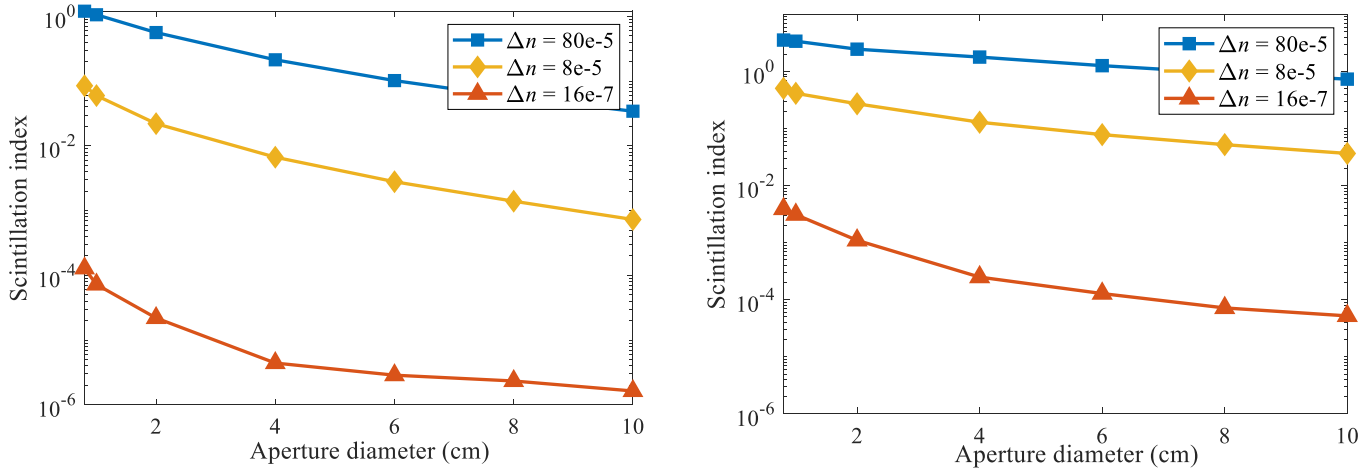

(a) (b)

Figure 4. SI vs. the Rx's aperture diameter for different vlaues of Δ*n:* (a) *L* = 30 m, and (b) *L* = 100 m

Fig. 5 illustrates the variations of SI against the Rx's FOV for different values of Δ*n* and for *L* = 30 m and 100 m. It can be inferred from Fig. 5 that, the effect of turbulence on the fluctuations of the photons angle of

arrival or angular spreading at the Rx is negligible. Therefore, increasing the Rx's FOV for L of 30 and 100 m has negligible effect on the SI except for lower values of FOV (i.e., < 0.2°) for L = 30 m and higher values of Δn for both L. Similar results were observed for longer link spans, which has not presented here.

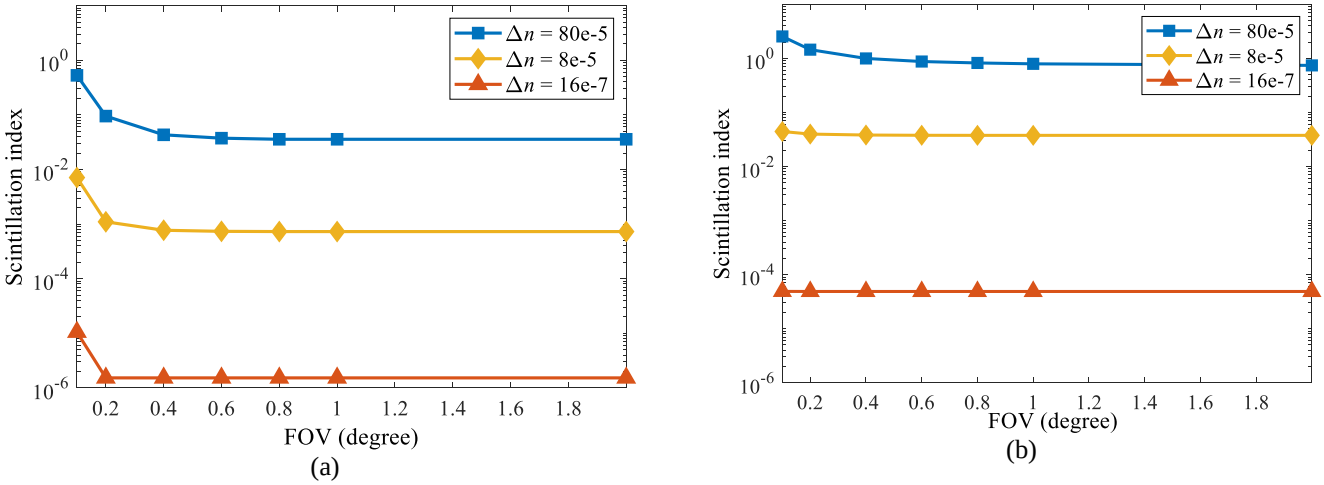

Figure 5. SI vs. the Rx's FOV for different vlaues of Δn for: (a) L = 30 m, and (b) L = 100 m

V. CONCLUSION

To investigate the effect of turbulence on UOWC link, not only the channel parameters but also the Tx and the Rx characteristics should be investigated. Both the link span and refractive index variations are the two main factors affecting the turbulence strength and hence the fluctuations of the received light intensity. While the effect of refractive index variations was studied in our previous works, in this paper based on our previously proposed turbulence model, we investigated the effect of link span (up to 150 m) on the PDF of the received light intensity for a constant value of refractive index variations. Simulation results showed that, lognormal and negative exponential distributions fitted well with the PDF of the received light intensity for weak-to-strong and saturated turbulence regimes, respectively. Performing goodness of fit test, it was shown that, the two mentioned distributions predicted the simulation results with coefficient of determination greater than 0.82 for all simulation results. In addition, the effect of the Tx's divergence angle, the Rx's aperture diameter and the FOV on the SI were investigated for a range of refractive index variations and link spans. It was shown that, the SI significantly reduced by increasing the Rx's aperture diameter, whereas increasing the Tx's divergence angle and the Rx's FOV had a negligible effect on the SI except for the small values of Tx's divergence angle and the Rx's FOV.

REFERENCES

[1] Z. Zeng, “A survey of underwater wireless optical communication.” University of British Columbia, 2015.

[2] C. Gabriel, M. A. Khalighi, S. Bourennane, P. Léon, V. Rigaud, Monte-Carlo-based channel characterization for underwater optical communication systems, J. Opt. Commun. Netw. 5 (2013) 1-12.

[3] S. Tang, Y. Dong, X. Zhang, Impulse response modeling for underwater wireless optical communication links, IEEE Trans. Commun. 62 (2014) 226-234.

[4] Z. Vali, A. Gholami, D. G. Michelson, Z. Ghassemlooy, M. Omoomi, H. Noori, Use of Gaussian beam divergence to compensate for misalignment of underwater wireless optical communication links, IET Optoelectron. 11 (2017) 171-175.

[5] Z. Vali, A. Gholami, Z. Ghassemlooy, M. Omoomi, Receiver Parameters Effect on Underwater Optical Wireless Communication Performance in the Presence of Transmitted Gaussian Beam, in 2018 11th CSNDSP, 2018, pp. 1-5.

[6] Z. Ghassemlooy, W. Popoola, S. Rajbhandari, Optical wireless communications: system and channel modelling with Matlab, CRC press, 2019.

[7] J. R. Potter, UComms: a conference and workshop on underwater communications, channel modeling, and validation, IEEE J. Oceanic Eng. 38 (2013) 603-613.

[8] M. V. Jamali, F. Akhoundi, J. A. Salehi, Performance characterization of relay-assisted wireless optical CDMA networks in turbulent underwater channel, IEEE Trans. Wirel. Commun. 15 (2016) 4104-4116.

[9] A. C. Boucouvalas, K. P. Peppas, K. Yiannopoulos, Z. Ghassemlooy, Underwater optical wireless communications with optical amplification and spatial diversity, IEEE Photonics Tech. L. 28 (2016) 2613-2616.

[10] Z. Vali, A. Gholami, Z. Ghassemlooy, D. G. Michelson, M. Omoomi, H. Noori, Modeling turbulence in underwater wireless optical communications based on Monte Carlo simulation, J. Opt. Soc. Am. A 34 (2017) 1187-1193.

[11] P. Yue, M. Wu, X. Yi, Z. Cui, X. Luan, Underwater optical communication performance under the influence of the eddy diffusivity ratio, J. Opt. Soc. Am. A 36 (2019) 32-37.

[12] E. Zedini, H. M. Oubei, A. Kammoun, M. Hamdi, B. S. Ooi, M. Alouini, Unified Statistical Channel Model for Turbulence-Induced Fading in Underwater Wireless Optical Communication Systems, IEEE Trans. Commun. (2019) 1-1.

[13] S. Kumar, S. Prince, J. Venkata Aravind, S. Kumar G, Analysis on the effect of salinity in underwater wireless optical communication, Mar. Georesour. & Geotec. (2019) 1-11.

[14] M. P. Bernotas, C. Nelson, Probability density function analysis for optical turbulence with applications to underwater communications systems, in Proc. of SPIE, 2016, pp. 98270D-98270D-10.

[15] W. Liu, Z. Xu, L. Yang, SIMO detection schemes for underwater optical wireless communication under turbulence, Photonics Research 3 (2015) 48-53.

[16] M. V. Jamali, P. Khorramshahi, A. Tashakori, A. Chizari, S. Shahsavari, S. AbdollahRamezani, et al., Statistical distribution of intensity fluctuations for underwater wireless optical channels in the presence of air bubbles, in IWCIT, Iran, 2016, pp. 1-6.

[17] S. A. Arpali, Y. Baykal, Ç. Arpali, BER evaluations for multimode beams in underwater turbulence, J. Mod. Opt. 63 (2016) 1297-1300.

[18] Z. Vali, A. Gholami, Z. Ghassemlooy, M. Omoomi, Investigation of Underwater Optical Wireless Communications with Turbulence, in 1st WACOWC, Iran, 2018.

[19] Z. Vali, A. Gholami, Z. Ghassemlooy, M. Omoomi, D. G. Michelson, Experimental study of the turbulence effect on underwater optical wireless communications, Appl. Opt. 57 (2018) 8314-8319.

[20] L. C. Andrews, R. L. Phillips, C. Y. Hopen, Laser beam scintillation with applications, SPIE press, 2001.

[21] V. V Nikishov, V. I. Nikishov, Spectrum of turbulent fluctuations of the sea-water refraction index, Int. J. fluid Mech. Res. 27 (2000).

[22] N. Farwell, Optical beam propagation in oceanic turbulence, University of Miami, 2014.

[23] S. A. Thorpe, An introduction to ocean turbulence, Cambridge University Press, 2007.

[24] L. Sun, J. Wang, K. Yang, M. Xia, J. Han, The research of optical turbulence model in underwater imaging system, Sensors & Transducers 163 (2014) 107.

[25] R. C. Millard, G. Seaver, An index of refraction algorithm for seawater over temperature, pressure, salinity, density, and wavelength, Deep Sea Res. Part A. Oceanogr. Res. Pap. 37 (1990) 1909–1926.

[26] S. Matt, W. Hou, W. Goode, S. Hellman, Velocity fields and optical turbulence near the boundary in a strongly convective laboratory flow, in Ocean Sensing and Monitoring VIII, 2016.

[27] I. E. Lee, Free space optical communication systems with a partially coherent Gaussian beam and media diversity, Northumbria University, 2014.

[28] A. K. Majumdar, J. C. Ricklin, Free-space laser communications: principles and advances, Springer science & business media, 2010.